Effects of energy density on the microstructure evolution of TiC/Ti6Al4V-ELI metal composite fabricated with laser metal deposition

Abstract. This study investigated the microstructural evolution of Ti6Al4V-ELI reinforced with TiC, fabricated via in-situ laser metal deposition technique. The 3.85% volume fraction TiC/Ti6Al4V-ELI metal composite samples were fabricated at two different energy densities (ED). It was observed that in-situ reaction resulted in various morphologies (unmelted or partially melted, chain-shaped eutectic, granular eutectic, granular primary eutectic, and dendritic primary) of TiC embedded with the beta grain boundary and the acicular alpha prime matrix. The size of dendritic structures decreases with respect to ED. Additionally, the hardness average of 457.59 ± 39.73 and 455.08 ± 18.03 $HV_{0.3}$ for 96 and 102 J/mm^2 ED respectively.

INTRODUCTION

Laser metal deposition (LMD) has attracted attention over the past years due to its inherent advantages, such as unrivaled design freedom and short lead times [1]. LMD is a complex technique influenced by numerous process factors, such as powder feed rate, laser power, and scanning speed. LMD technique provides the flexibility of feeding different materials required to produce a titanium matrix composite (TMC). LMD has been used to produce clad with a superior material or composite matrix. It is also reported in the literature [2 -4] that the material with superior properties is partially melted, in an attempt to retain its physical property.

LMD, as a novel material surface modification technology, has the advantages of a shorter preparation time, stable quality, and good interface combination, as well as the avoidance of cracks induced by thermal effects, when compared to traditional surface modification technology [5 - 6]. Cui et al. discovered that a Ti/7YSZ composite coating created using the LMD process increased the wear resistance of the TC4 titanium alloy [7]. The findings demonstrate that at different laser scanning rates, the microstructure of the Ti-based composite thermal barrier coating system changed from top to bottom [7]. Wang et al., [8] fabricated TiC/Ti6Al4V composites with varied Y element concentrations. The influence of Y content on the microstructure and mechanical properties of composites was studied [8]; however, the new material's integrity was weak, and its interaction with the matrix was poor. The reinforcing phase produced by the in-situ reaction approach, on the other hand, was finer and more stable, with a high bonding strength to the matrix. As a result, this approach has gotten a lot of attention [9]. LMD was also used to fabricate Ti/SiC and in-situ TiN dendrite-reinforced composite coatings on a Ti6Al4V substrate using a combined powder of C and Si and the laser nitriding process [10 – 11]. However, there are few publications on LMD of

TiC/Ti6Al4V composites with totally melted TiC. The results of a study on fully melted TiC reinforced titanium matrix composites with LMD are useful for future research. These composites can handle the increased demands of rapidly emerging high-tech areas including aviation, aerospace, electronics, and automobiles, extending their engineering applications in particular.

In this study, TiC/Ti6Al4V-ELI matrix composite was fabricated with LMD processes at two different energy densities (ED), using Ti6Al4V-ELI and TiC powders to get a 3.85% TiC volume ratio fraction to Ti6Al4V-ELI. The formation mechanism of primary and eutectic TiC was studied together with the microstructure evolution and microhardness of the TiC/Ti6Al4V-ELI matrix composite. In addition, the influence of primary and eutecticTiC on the microhardness of TiC/Ti6Al4V-ELI is discussed.

METHODOLOGY AND RESULTS

Materials

A spherical grade 23, pre-alloyed Ti6Al4V ELI powder with particle size distribution in the range of 45 – 100 µm (supplied by TLS Technik GMbH & Co, Bitterfeld, Germany) was used as the matrix. A TiC powder with particle size in the range -140+325 mesh (supplied by Stanford Advance Material) was used as a reinforcing material. The morphologies of the Ti6Al4V-ELI and TiC powders are shown in Fig. 1.
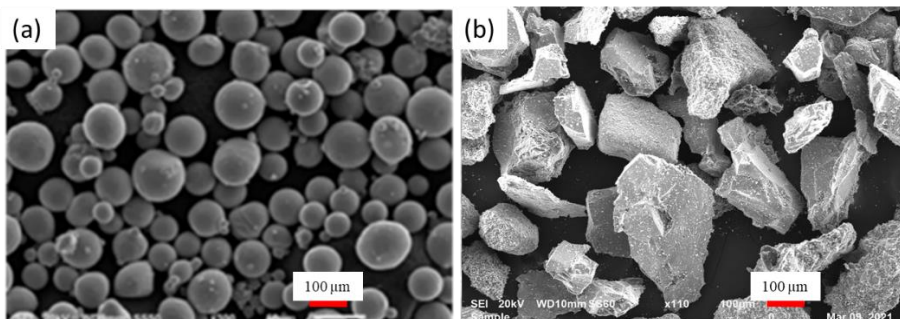

Fig. 1: SEM images of the powders (a) Ti6Al4V-ELI, (b) TiC.

The Ti6Al4V-ELI showed spherical and smooth particles, with no porosity as can be seen in Fig. 1(a). Spherically shaped and smooth Ti6Al4V ELI particles were reported in other studies [12 – 13]. On the other hand, Fig. 1(b) TiC powder revealed coarse irregular-shaped particles. Irregular-shaped particles of TiC were also reported in the literature [13]. The samples were deposited on an acetone rinsed Ti6Al4V base plate, which was used as the substrate.

Method

All samples were manufactured on an IPG fibre laser (1073nm wavelength) processing system which was integrated with a KUKA robot and a 3-way nozzle. A GTV powder system (D-57629), equipped with two powder feed hoppers was used to deliver the Ti6Al4V-ELI and TiC powders through the carrier gas during deposition. The powder flow rate for Ti6Al4V-ELI was fixed at 5.0 rpm, and TiC at 0.3 rpm. The powder carrier gas was blown

at 1.5 l/min during the deposition process. Argon gas was used as a shielding gas to prevent oxidation on the manufactured samples. Laser power was varied for each deposition at 1600, and 1700 W. The following process parameters were maintained during deposition of samples, scanning speed of 0.5 m/min, gas flow rate of 12 l/min, and beam diameter of 2 mm. The Ti6Al4V base plate was subjected to sandblasting to prepare it for deposition. Long single-line tracks of approximately 40 mm with 50% layer overlap in the y-direction were deposited. Fig. 2 below shows a schematic diagram of LMD.
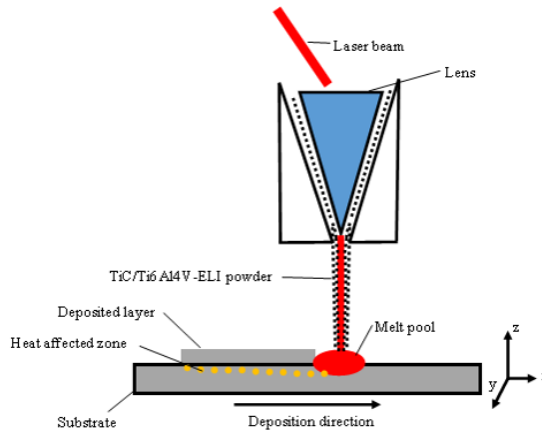

Fig. 2: Schematic diagram of LMD

The deposited samples were cut perpendicular to the deposition direction on a Struers Labotom-5 cutting machine using a Struers high-quality titanium cut-off wheel (20S25). The samples were then mounted using an AMP 50 automatic mounting press machine. AKA Resin Phenolic SEM black conductive resin was used to mount all samples. The mounted samples were mechanically ground with Struers Tetrapol-25 grinding and polishing machine. Silicon carbide (SiC) grinding papers with grit sizes of 80, 320, 1200, and 4000 were used for grinding the samples which were later surface finished by polishing to a mirror finish using Diapro MD-Mol 3 µm diamond suspension and colloidal silica 0.04 µm OP-S suspension for 3 min. The specimens were etched with Kroll's reagent, a solution containing 100 ml H_2O, 1-3 mL HF, and 2-6 mL HNO_3. The metallographically prepared and etched, samples were observed for microstructure using a Joel JSM-6010PLUS/LA scanning electron microscope fitted with electron dispersive spectrum (SEM/EDS). Hardness measurements were performed using the Matsuzawa Seiko Vickers model MHT-1 micro-hardness machine. All measurements were done using a diamond type of indenter and applying a force of 0.3 kgf and a dwell time of 10 seconds. For all samples, three hardness patterns were measured, and the average was calculated as the hardness of the material.

Microstructure analysis

Fig. 3 below shows the SEM microstructure images of the 3.85% vol. fraction of TiC/Ti6Al4V-ELI fabricated with LMD at two different ED. The microstructures were observed in the Y direction as indicated in Fig. 3. Fig. 3(a) shows the microstructure of 96 J/mm^2 and Fig. 3(b) shows the microstructure of 102 J/mm^2. In Fig. 3(a) chain-shape and veins of TiC are observed along the overlap zone and distributed in the prior beta grain boundaries. Granular eutectic particles are observed where layer remelting occurred. In a study by Li et al. [2] it is reported that the addition of TiC to the titanium matrix lead to solid

solution strengthening by the resulting TiC morphologies. The presence of blocky or partially melted TiC observed near the columnar to equiaxed transition zones is attributed to the Marangoni flow effect [14]. In a study by Antony and Arivazhagan [14] reports that negative surface tension tent to pull the liquid metal away from the melt pool, thus leaving TiC particles with insufficient ED required to dissolve. Fig. 3(b) shows granular eutectic and veins of TiC distributed homogeneously across the matrix. Chain-shaped TiC is observed alongside the columnar prior-beta grain boundary. The TiC morphologies observed in fig. 3(b) where also reported in literature by Li et al. [15]. The size and presence of the granular eutectic TiC observed in the matrix indicate sufficient ED to completely dissolve TiC particles.
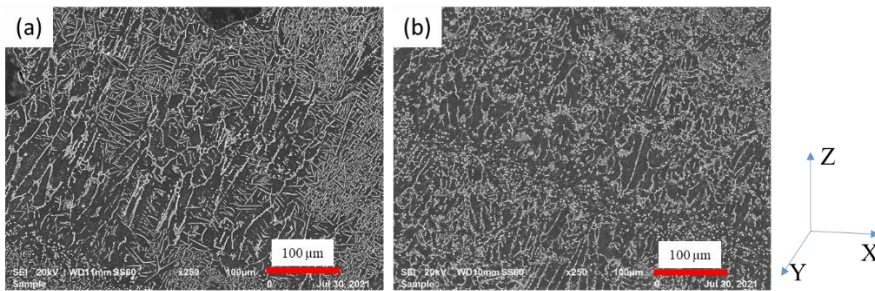

Fig. 3: SEM microstructures of 3.85 % vol. fraction TiC/Ti6Al4V-ELI fabricated at energy densities of (a) 96 J/mm^2 and (b) 102 J/mm^2 observed in the Y-direction.

Fig. 4 shows the microstructure obtained from the first and last layer (total of five layers were deposited), which is not affected by the overlap effect. It is observed that by increasing the energy density from Fig. 4(a) 96 J/mm^2 to Fig. 4(b) 102 J/mm^2 complete melting was achieved. It is also observed that the TiC morphology is homogeneously distributed across the matrix. Wang et al. [16] reported that the chain-shape distribution was mostly eutectic TiC. This reported morphology is attributed to the eutectic transformation of TiC/Ti6Al4V-ELI during solidification as reported by Zhou et al. [17].
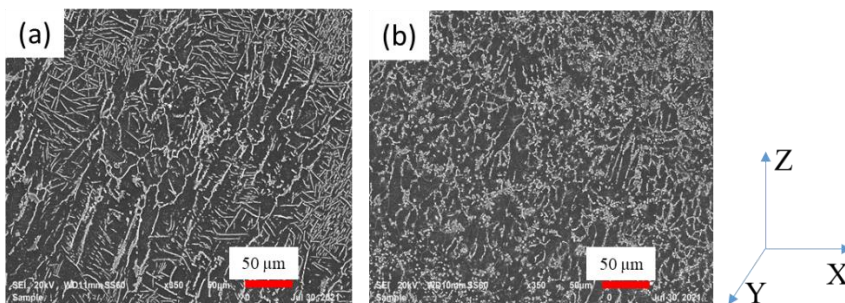

Fig. 4: SEM microstructure of 3.85% vol. fraction TiC/Ti6Al4V-ELI fabricated at energy densities of (a) 96 J/mm^2 and (b) 102 J/mm^2 observed in the Y-direction.

Micro-hardness

Fig. 5 below shows the Vickers micro-hardness of 3.85 % vol. fraction of TiC/Ti6Al4V-ELI fabricated with (a) 96 J/mm^2 and (a) 102 J/mm^2. In plot (a) the hardness shows an increasing exponentially from the substrate through to the clad layer. The clad starts from the depth of 400 to 1200 µm. From the depth of 400 to 800 µm hardness plot shows a relatively linear

plot. At a depth of 900 to 1100 µm there are fluctuations in the plot. These fluctuations are due to the partially melted TiC particles as indicated in Fig. 3(a). Fig. 5(b) shows an increasing linear plot in the substrate and the heat-affected zone (HAZ) or the interface at the depth of 0 to 400 µm. The clad zone (400 to 1200 µm) indicates a linear plot with an average hardness of 472.11 ± 20.19 $HV_{0.3}$. At a depth of 1100 µm hardness peaks at 501 $HV_{0.3}$, this is due to the refined grain size as a result of convection cooling. The hardness plot of fig. 5(b) correspond with the microstructure shown in fig. 3(b) and 4(b).
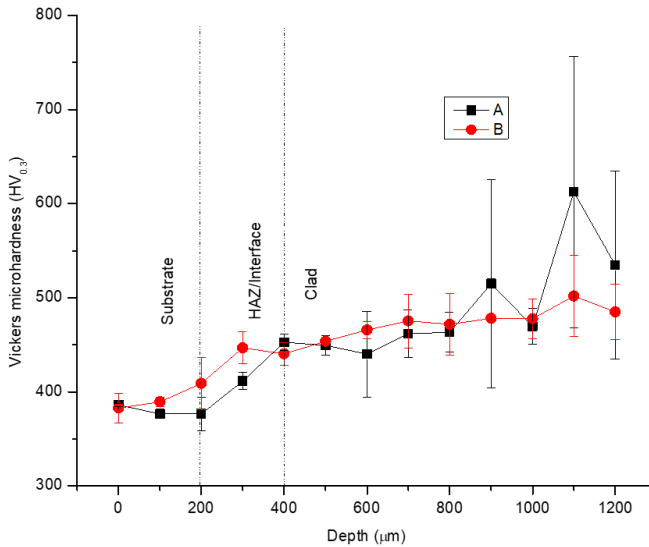

Fig. 5: Vickers micro-hardness of 3.85 % vol. fraction TiC/Ti6Al4V-ELI fabricated at energy densities of (A) 96 J/mm^2 and (B) 102 J/mm^2.

CONCLUSION

In-situ synthesis of TiC and Ti6Al4V-ELI with the LMD technique was accomplished and melting of TiC was possible. TiC particles are homogenously distributed in the beta grain boundary and the acicular alpha prime matrix. The observed morphologies of the second phase particle are eutectic granular, primary granular, primary dendrite and blocky or partially melted TiC. By increasing the energy density from 96 to 102 J/mm^2, the TiC particles were completely dissolved in the matrix. Samples produced at a higher energy density showed a homogenous distribution of reinforcing particles. The hardness average of 457.59 ± 39.73 and 455.08 ± 18.03 $HV_{0.3}$ for 96 and 102 J/mm^2 ED respectively.

REFERENCES

[1] J. Kranz, D. Hertzog and C. Emmelmann, "Design guidelines for laser additive manufacturing of light structures in Ti6Al4V," *Journal of Laser Application,* 2015.

[2] L. Li, J. Wang, P. Lin and H. Liu, "Microstructural and mechanical properties of functionally graded TiC/Ti6Al4V composite fabricated by laser melting deposition," *Ceramics International,* vol. 43, pp. 16638-16651, 2017.

[3] N. K. K. Arthur, C. Siyaya, S. Pityana and M. Tlotleng, "Microstructural response of Ti6Al4V-ELI alloyed with molybdenum by direct energy deposition," *Journal of materials engineering and performance,* vol. 30, no. 7, pp. 5455-5465, 2021.

[4] J. Qi, H. H. Wang, C. M. Zou and Z. J. Wei, "Influence of matrix characteristics on tensile properties of in-situ synthesized TiC/TA15 composite," *Materials Science Engineering,* vol. A 553, pp. 59-66, 2012.

[5] F. Weng, H. Yu, C. Chen, J. Liu and L. Zhao, "Microstructures and properties of TiN reinforced Co-based composite coatings modified with Y2O3 by laser cladding on Ti6Al4V alloy," *Journal of Alloys and Compounds,* vol. 650, pp. 178-184, 2015.

[6] Q. Meng, L. Geng and D. Ni, "Laser cladding NiCoCrAlY coating on Ti6Al4V," *Materials Letters,* vol. 59, no. 22, pp. 2774-2777, 2005.

[7] J. Cui, W. Zhai, M. K. Lu, H. Zhang, M. Pang and G. F. Yang, "Experimental study of the microscopic characteristics of Ti-based laser cladding Ti+7YSZ composite thermal barrier coatings," *Optik,* vol. 208, p. 164087, 2020.

[8] X. Wang, X. Ma, Q. Nie and M. Wang, "Effects of Y addition on microstructure and mechanical properties of TiC/Ti6Al4V composite," *Intermetallics,* vol. 31, pp. 242-248, 2012.

[9] Y. Lei, R. Sun, J. Lei, Y. Tang and W. Niu, "A new theoretical model for high power laser clad TiC/NiCrBSiCcomposite coating on

Ti6Al4V alloys," *Optics and lasers in engineering,* vol. 48, no. 9, pp. 899-905, 2010.

[10] P. Jiang, X. L. He, X. A. Li, L. Yu and H. Wang, "Wear resistance of a laser surface alloyed Ti6Al4V alloy," *Surface and Coatings Technology,* vol. 130, no. 1, pp. 24-28, 2000.

[11] Y. Tian and C. Z. Chen, "Microstructure and wear propertie of in situ formed composite coatings produced by laser alloying technique," *Materials Letters,* vol. 61, no. 3, pp. 635-638, 2007.

[12] Z. Zhou, Y. Liu, Q. Zhan and K. Wang, "Microstructure evolution and mechanical properties of in-situ Ti6Al4V-TiB composites manufactured by selective laser melting," *Composites part B: Engineering,* vol. 207, p. 108567, 2021.

[13] P. Ramasobane, P. M. Mashinini and B. N. Masina, "In-situ synthesis ofTiC/Ti6-Al-4V-ELI composite by laser," *South African Journal for Science and Technology / Suid-Afrikaanse Tydskrif vir Natuurwetenskap en Tegnologie,* vol. 40, pp. 70-74, 2021.

[14] K. Antony and N. Arivazhagan, "Studies on energy penetration and marangoni effect during laser melting process," *Journal ngineering Science and Technology,* vol. 10, no. 4, pp. 509-525, 2015.

[15] L. Li, J. Wang, P. Lin and H. Liu, "Microstructural and mechanical properties of functionally 204 garded TiC/Ti6Al4V composite fabricated by laser melting deposition," *Ceramics International,* pp. 16638-16651, 2017.

[16] J. D. Wang, L. Q. Li, C. W. Tan, H. Liu and P. P. Lin, "Microstructure and Tensile Properties of TiCp/Ti6Al4V Titanium Matrix Composites Manufactured by Laser Melting Deposition," *Journa of Material Processing Technology,* vol. 252, pp. 524-536, 2018.

[17] B. Ya, B. W. Zhou, H. S. Yang, B. K. Huang, F. Jia and X. G. Zhang, "Microstructure and mechanical properties of in situ casting TiC/Ti6Al4V composites through adding multi-walled carbon nanotubes," *Journal of Alloys and Compounds,* vol. 637, pp. 456-460, 2015.